J. Fluid Mech. (2014), *vol.* 755, *pp.* 485–502.
doi:10.1017/jfm.2014.429

Taylor bubble rising in a vertical pipe against laminar or turbulent downward flow: symmetric to asymmetric shape transition

Jean Fabre[1,†] **and Bernardo Figueroa-Espinoza**[2]

[1]Institut de Mécanique des Fluides, Institut National Polytechnique de Toulouse, Allée du Professeur Camille Soula, 31400 Toulouse, France

[2]Instituto de Ingeniería, Universidad Nacional Autónoma de México, Calle 21 No. 97A, Colonia Itzimná, 97100, Mérida, Mexico

(Received 12 April 2014; revised 13 June 2014; accepted 22 July 2014; first published online 20 August 2014)

The symmetry of Taylor bubbles moving in a vertical pipe is likely to break when the liquid flows downward at a velocity greater than some critical value. The present experiments performed in the inertial regime for Reynolds numbers in the range $100 < Re < 10\,000$ show that bifurcation to an eccentric motion occurs, with a noticeable increase of the bubble velocity. The influence of the surface tension parameter (an inverse Eötvös number), Σ, has been investigated for $0.0045 < \Sigma < 0.067$. It appears that the motion of an asymmetric bubble is much more sensitive to surface tension than that of a symmetric bubble. For any given Σ, the symmetry-breaking bifurcation occurs in both laminar and turbulent flow at the same vorticity-to-radius ratio $(\omega/r)_0$ on the axis of the carrier fluid. This conclusion also applies to results obtained previously from numerical experiments in plane flows.

Key words: bubble dynamics, drops and bubbles, gas/liquid flows

1. Introduction

Taylor bubbles moving in a vertical pipe become asymmetric when the surrounding liquid flows downward at a mean velocity greater than some critical value. The tip of the long bullet-shaped bubbles moves into an eccentric position, and the resulting asymmetric bubbles move faster, relative to the liquid, than symmetric bubbles. This has a significant influence in slug flow where most of the gas is carried in a series of long bubbles and this is why symmetry breaking was first observed in such flow conditions. In their study of upward and downward slug flow Griffith & Wallis (1961) noted that 'as the down flow water velocity was increased, a point was reached at which the stable character of the bubble suddenly changes; the tip of the bubble began to distort to become alternately eccentric on one side or another'. Fifteen years later Martin (1976) focused on downward slug flow. His experimental results showed that 'a stable Taylor bubble is only possible in downward flow for large values of the surface tension' and that 'the bubbles become more and more eccentric as the downward flow

† Email address for correspondence: Jean.Fabre@imft.fr

is increased'. However these studies were performed in slug flow and one cannot exclude the possibility that the motion and shape of each bubble were modified by those of the preceding bubble. Our understanding of the dynamics of an individual Taylor bubble (as opposed to a train of bubbles) in liquid flowing in vertical pipes was advanced by Nicklin, Wilkes & Davidson (1962), who obtained a correlation between the bubble velocity V, the mean liquid velocity U, the pipe diameter D and the gravitational acceleration g. Their correlation,

$$V = C_0 U + C_\infty \sqrt{gD}, \tag{1.1}$$

valid for the inertial regime and confirmed later by the theories of Collins *et al.* (1978) and of Bendiksen (1985), became the cornerstone of slug flow models. It suggests that the bubble velocity V depends on the uncoupled effects of liquid transport and buoyancy. In (1.1) C_0 and C_∞ are two dimensionless coefficients that may depend on the Reynolds number $Re = UD/\nu$, the surface tension parameter (an inverse Eötvös number) $\Sigma = 4\sigma/\rho g D^2$, and the viscosity parameter $N_\nu = \nu/(gD^3)^{1/2}$, where ρ is the liquid density, ν the liquid kinematic viscosity and σ the surface tension (e.g. Fabre & Liné 1992). Although Nicklin *et al.* (1962) paid little attention to bubbles in downward flow, they noted that these bubbles behave as in slug flow by adopting 'a wedge shape, in an attempt to avoid the fast moving liquid in the centre of the tube'.

The dynamics of Taylor bubbles in downward flow were apparently ignored until Lu & Prosperetti (2006) attempted to throw some light on this issue. They performed a stability analysis of the bubble shape assuming zero surface tension, and demonstrated that there exists in Poiseuille flow a critical mean velocity $U_c \approx -0.13(gD)^{1/2}$ below which (i.e. for $U < U_c < 0$) the bubble is unstable to small irrotational perturbations. They argued that the instability occurs because the relative velocity between the bubble and the liquid decreases with increasing downflow, resulting in a flattening of the bubble tip.

Figueroa-Espinoza & Fabre (2011) recently reported two-dimensional numerical experiments on plane Taylor bubbles moving in vertical Poiseuille flow. They observed that below a critical mean liquid velocity, a transition to a non-symmetric, faster-moving, bubble occurs. They also showed that surface tension has a stabilizing effect on the transition by decreasing the critical velocity (i.e. by increasing $|U_c|$). Carrying on from this numerical study, the present laboratory experiments investigate the motion and the shape of Taylor bubbles rising in vertical pipes against downward liquid flows and quantify the contribution of surface tension. They were performed in two constant-volume rigs that allowed measurement of the bubble velocity and observation of its shape (§ 2). Whereas the numerical experiments were limited to laminar flow, the present results have been obtained in both laminar and turbulent flows (§ 3). The results from the plane and axisymmetric geometries can be unified by the choice of the right bifurcation parameter (§ 4).

2. Experimental facilities

Previous theoretical studies in vertical pipe flow (e.g. Collins *et al.* 1978; Bendiksen 1985) have shown the importance of the velocity profile of the flowing liquid on the bubble motion: for example, $C_0 \approx 2$ or 1.2 according to whether the flow is laminar or turbulent. Therefore, the bubble velocity and shape have to be determined in conjunction with the velocity profile. In view of these two objectives we chose to use

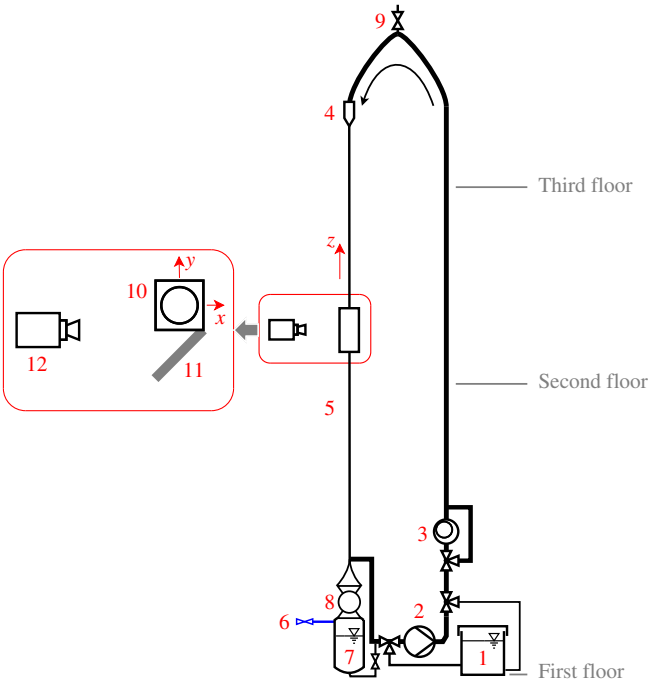

FIGURE 1. (Colour online) Experimental facility: 1, reservoir; 2, progressing cavity pump; 3, positive displacement flowmeter; 4, anti-swirl and honeycomb; 5, test section; 6, air inlet; 7, vessel; 8, ball valve followed by a convergent; 9, air vent; 10, visualization box; 11, mirror; 12, HSV camera.

optical methods: particle image velocimetry (PIV) for characterizing the liquid flow far ahead of the bubble, and high-speed video (HSV) to record the bubble shape and velocity. For the velocity measurements to be accurate, the gas expansion that would occur if bubbles ascended in an unpressurized rig must be avoided. This implies that a closed loop is required to produce bubbles of constant volume. To investigate the influence of the surface tension parameter Σ over as wide a range as possible, two different loops were used.

The larger facility, designed for 40 and 80 mm diameter pipes and of total height 12.3 m, is shown schematically in figure 1. A water–glycerol mixture initially prepared in a reservoir (1) was recirculated by one of the two progressing cavity pumps (2) that produced flow rates over the range 70–3000 l h^{-1}. The mixture flowed up to the topmost section through a vertical pipe of 80 mm internal diameter. It passed through a positive displacement flowmeter (3) that gave the flow rate to an accuracy of ± 1 % in the range 120–9000 l h^{-1} and was calibrated outside this range by timing the filling of the 80 mm pipe up to a given height. The water–glycerol mixture then flowed down through an elbow that contained an anti-swirl and a honeycomb (4): these two devices were designed to reduce the development distance by counteracting flow asymmetry and large eddies that were generated by the preceding elbows. The test section (5) consisted of a 9 m long Plexiglas pipe that could be changed to allow different diameter pipes to be used. For each run a given volume of air (6) was introduced into a vessel (7) of 160 mm diameter closed at its top by a ball valve (8) of the same diameter. Then the air vent (9) was closed. While the pump

Fluid	Glycerol (%)	Viscosity (mPa s)	Density (kg m^{-3})	Surface tension (N m^{-1})
Water	0	1.0	1000	0.072
Mixture 1	40	3.5	1096	0.048
Mixture 2	55	5.6	1126	0.045

TABLE 1. Physical properties of water–glycerol mixtures at $20 \pm 1\,^{\circ}$C.

was operating, the ball valve was quickly opened and the trapped air escaped from the vessel through the convergent, generating a Taylor bubble that rose in the test section as long as the adverse liquid flow rate was not too large. When the bubble reached the top of the loop, the air vent was again opened and a new run could start. The optical systems, PIV and HSV, were located 3.5 m downstream of the honeycomb. To reduce the distortion due to optical refraction, we used a transparent parallelepiped-shaped box (10), 50 cm high and 15 cm wide, filled with the same water–glycerol mixture. By using a mirror (11) at 45°, the HSV (12) captured two side-by-side views simultaneously: the front and the side views referred to as the x- and y-views (see figure 1). The y-view had to be rescaled numerically to account for the longer optical path that led from the object to the camera via the mirror. For the box illumination, LED backlight units were used to avoid shadows and reflections. The recorded movies, with time-marked images, were used to determine the bubble velocity.

To extend the range of the surface tension parameter we designed a smaller rig that used a 20 mm diameter pipe. This second loop was a 4 m high copy of the previous, larger loop, with some minor differences: the volumetric pump was replaced by a centrifugal one and the flow rates were measured with rotameters in the range 16–170 l h^{-1}.

In both facilities we used three different water–glycerol mixtures the properties of which are given in table 1. The viscosity was measured with a cone-and-plate viscometer and the surface tension was determined by means of a Wilhelmy plate tensiometer. As will become clear, these different mixtures were used mainly in order to increase the fluid viscosity so as to extend the laminar domain. They offered less scope for changing the surface tension, which could at best be halved.

To verify the symmetry of the velocity profile and to identify the range of the Reynolds number over which the laminar–turbulent transition occurs, PIV measurements were performed in the 40 mm pipe in the absence of any bubble. The light sheet in the visualization box was positioned in the diametral plane that cut both the pipe and the elbows, i.e. the plane where asymmetry might be observed. The measurements were performed using water and mixture 1 with different inlet systems: either honeycomb, anti-swirl, or both. An example of a velocity distribution is given in figure 2(a) for a Reynolds number corresponding to laminar flow: the asymmetry of the profile is almost indiscernible. To summarize the PIV results we plot in figure 2(b) the maximum-to-mean velocity ratio u_0/U together with the values this ratio takes for the range of the Reynolds number under consideration: 2 for the laminar regime and $(\log_{10} Re + 0.31)/(\log_{10} Re - 0.74)$ for the turbulent regime (appendix A). The present results show that the flow is laminar for $Re < 2000$ whereas it is turbulent for $Re > 5000$. In between there exists an intermediate region corresponding to the laminar–turbulent transition.

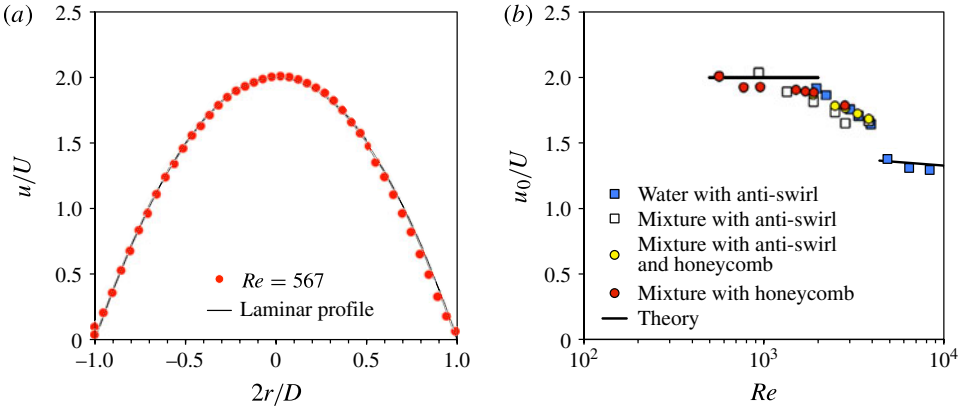

FIGURE 2. (Colour online) Results of PIV. (*a*) Velocity distribution. (*b*) Maximum-to-mean velocity ratio.

3. Experimental results

Single bubbles of given volume were released into liquid flowing at velocity U. Each bubble is characterized by its equivalent length L, i.e. the length of a cylinder of diameter D of the same volume. Note that L is smaller than the bubble length and that, as shown below, the velocity of a bubble of length $L > D$ is independent of its length.

Selected images of each movie were processed by using the Canny (1986) edge detection method to determine the polynomial approximation of the x- and y-contours of the bubble pictured in the x- and y-views. For an asymmetric bubble, the only coordinates of the bubble surface that can be unambiguously identified in these contours are those of the tip, e_x and e_y. In consequence, it was not possible to determine the radius of curvature of the bubble. The x- or y-contour may be viewed as the orthographic projection of the bubble on the planes $x = 0$ or $y = 0$ that pass through the tip. As such it is not necessarily identical to the cross-section of the bubble in the planes $x = 0$ or $y = 0$. This can be demonstrated by approximating the bubble surface in the vicinity of the tip by the second-order Taylor series $z = ax^2 + 2bxy + cy^2$: terms of higher order can be ignored since they play no role in the determination of the radii of curvature. The equations in the x- and y-planes are $z = cy^2$ and $z = ax^2$ whereas the equations of the orthographic projections are $z = (c - b^2/a)y^2$ and $z = (a - b^2/c)x^2$. The bubble mean curvature is $a + c$, but an attempt to determine the curvature from the projections would erroneously lead to $(a + c)(1 - b^2/ac)$, which is correct only for the improbable case $b = 0$, i.e. when the bubble is oriented such that it is symmetric with respect to one of the two planes. Thus we determined the radius of curvature R at the tip only for symmetric or quasi-symmetric bubbles.

From here on, dimensionless quantities will be used: $L^* = L/D$ for the equivalent length, $e^* = 2(e_x^2 + e_y^2)^{1/2}/D$ for the eccentricity, $R^* = 2R/D$ for the mean radius of curvature at the tip, $U^* = U/\sqrt{gD}$ for the liquid velocity and $V^* = V/\sqrt{gD}$ for the bubble velocity.

Preliminary experiments were carried out in the 40 mm pipe with water. The corresponding results are shown in figure 3 for bubbles of equivalent length $L^* = 3.33$. Here and in the following similar figures, each data point corresponds to a single

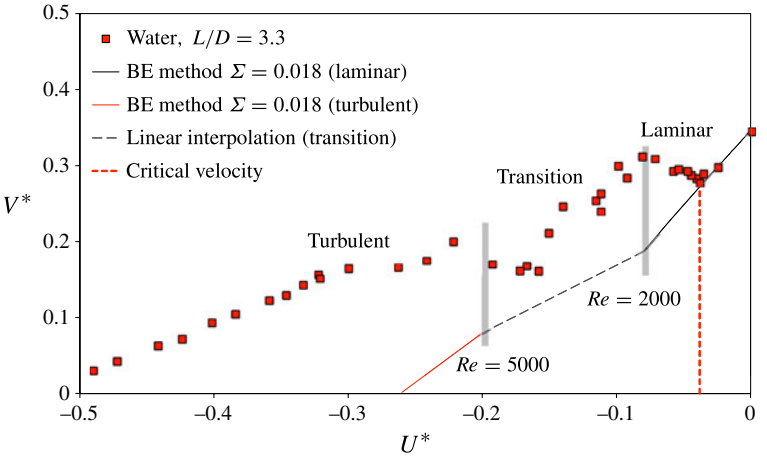

FIGURE 3. (Colour online) Bubble velocity in 40 mm pipe for water ($\Sigma = 18 \times 10^{-3}$, $N_v = 40 \times 10^{-6}$).

bubble. The two vertical grey lines delimit the transition region between laminar and turbulent regimes. The solid lines are the numerical predictions (see appendix A) obtained in laminar and turbulent regimes for a symmetric bubble by the boundary element (BE) method of Ha Ngoc & Fabre (2006), whereas the dashed line is estimated, in the transition region, from a linear interpolation. As a preliminary remark, the results appear slightly scattered, except in the laminar region. In fact the velocity measurements made by timing the motion of the bubble over the box height were not sufficiently accurate: the bubble velocity experienced small fluctuations about the average due to the shape fluctuations near the tip. Nicklin *et al.* (1962) made a similar observation: 'the unsteadiness in the region of down flow was shown by the wide variation in C_0 when this parameter was obtained by timing a slug over a short distance'. In the experiments that followed, the velocity was determined by timing the bubble motion over 2 m.

In the laminar region of figure 3, the bubble behaviour depends on whether U^* is greater or smaller than the critical velocity $U_c^* = -0.038$. If $U^* > U_c^*$ the bubble remains symmetric, as in still liquid, and its velocity is in good agreement with the numerical results of appendix A. If $U^* < U_c^*$, the bubble becomes asymmetric and it moves faster than anticipated. In the turbulent region the bubble velocity is clearly greater than that predicted for a symmetric bubble. In the transition region, u_0/U continuously evolves with the Reynolds number (see figure 2*b*) so that it is impossible to draw firm conclusions.

These experiments demonstrate the need to increase (resp. decrease) the viscosity or decrease (resp. increase) the diameter, in order to investigate the bifurcation in laminar (resp. turbulent) flow.

3.1. *Experiments in the laminar regime*

Two sets of experiments were carried out in the laminar regime: one set in a 40 mm pipe with water, mixture 1 or mixture 2, and the other in a 20 mm pipe with water or mixture 2.

The results in the 40 mm pipe are shown in figure 4: they are presented as two graphs, one for the velocity, the other for the eccentricity. For the sake of clarity

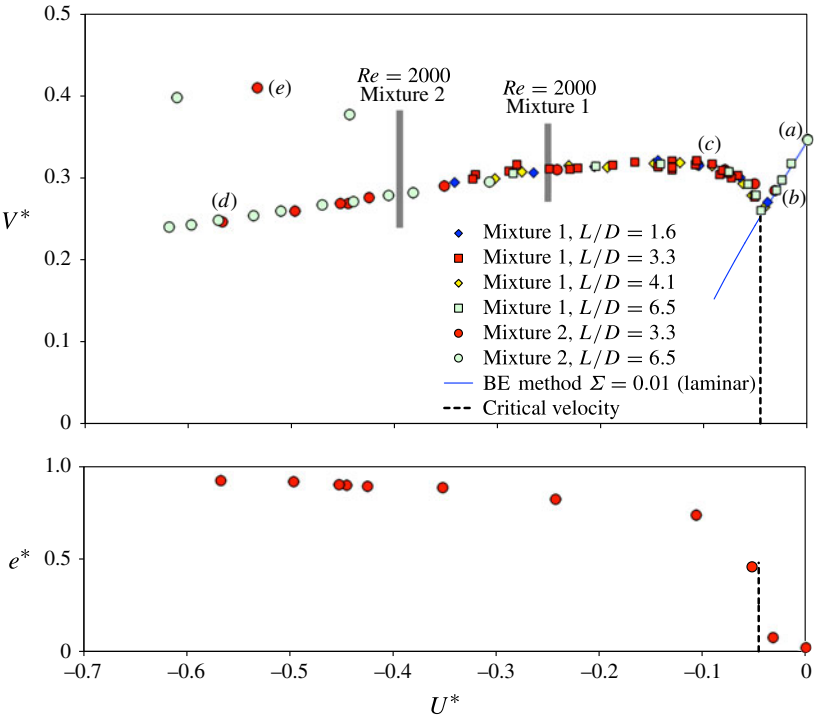

FIGURE 4. (Colour online) Bubble velocity and eccentricity in 40 mm pipe for mixture 1 ($\Sigma = 10.2 \times 10^{-3}$, $N_v = 126 \times 10^{-6}$) and mixture 2 ($\Sigma = 10.3 \times 10^{-3}$, $N_v = 197 \times 10^{-6}$).

the experiments with water, already shown in figure 3, have been removed. Let us leave aside for the moment the three points corresponding to $V^* \approx 0.4$: these will be discussed later. Bubbles of various equivalent lengths ($L^* = 1.6$, 3.3, 4.1, 6.5) were released and no velocity difference was observed apart from measurement uncertainty. In fact the velocity of a long symmetrical bubble is independent of its length as long as it is larger than approximately D. This somewhat counter-intuitive result can be explained by the fact that the surface waves are swept down by the supercritical-like flow of the falling film: thus the bottom of the bubble cannot influence the motion of its tip. The results of figure 4 show that the length independence is also true for asymmetric bubbles of length $L^* > 1.6$. Moreover, no significant difference was observed between mixtures 1 and 2 since Σ is approximately the same. Since the ratio N_{v2}/N_{v1} between these mixtures is approximately 1.6, one can state that viscosity has no observable influence. As in the experiments with water, two velocity regimes were observed according to whether U^* is larger or smaller than the critical velocity $U_c^* = -0.045$. The first, symmetric regime is again in good agreement with the numerical simulations performed in inviscid flow (appendix A): for this regime e^* should be strictly zero but a small eccentricity may be observed, as for the flow condition (b) of figures 4 and 5. The second regime corresponds to the asymmetric regime of faster-moving bubbles whose eccentricity increases with increasing downflow. It must be noted that the steep rise in velocity near U_c^* is concomitant with the steep rise in eccentricity. Examples of shape and motion of bubbles corresponding to the flow conditions of figure 4 are displayed in figure 5 and in online supplementary movie 1 (available at http://dx.doi.org/10.1017/jfm.2014.429). The bubbles are smooth and their tip stable, unlike their rear. As the downflow

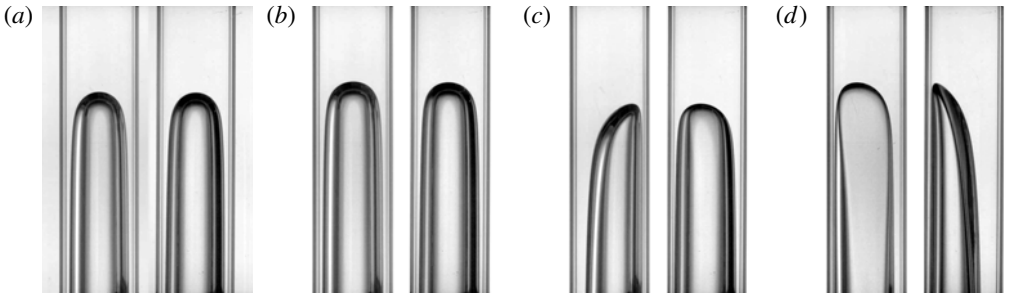

FIGURE 5. Bubble shape for the flow conditions of points (*a–d*) of figure 4.

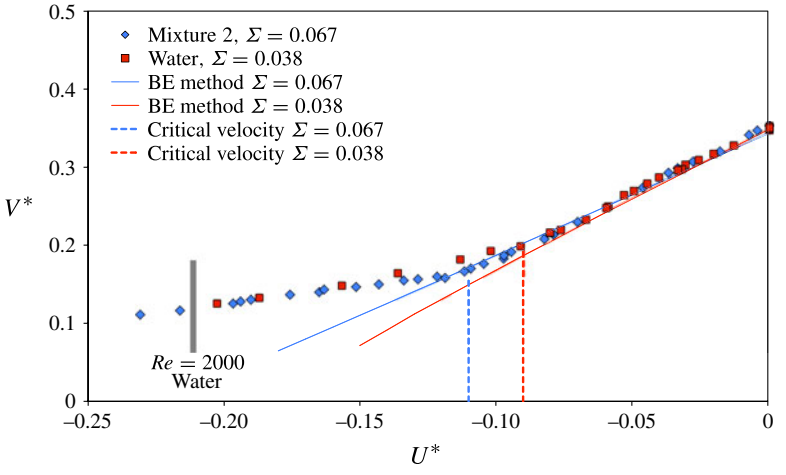

FIGURE 6. (Colour online) Bubble velocity in 20 mm pipe for water ($\Sigma = 67 \times 10^{-3}$, $N_\nu = 106 \times 10^{-6}$) and mixture 2 ($\Sigma = 38 \times 10^{-3}$, $N_\nu = 526 \times 10^{-6}$).

is increased an evolution of the bubble curvature is observed: while the bubble of figure 5(*c*) is apparently convex everywhere, that of figure 5(*d*) has a convex side shaped by the pipe whereas the other side is concave.

Results obtained in the 20 mm pipe are given in figure 6 for water and for mixture 2 (preferred to mixture 1 because it leads to a wider *Re*-range). Apart from the transition from a quasi-symmetric to asymmetric shape ($U_c^* = -0.11$ for the mixture, $U_c^* = -0.09$ for water), there is little difference between the two fluids. But differences compared to results obtained in the 40 mm pipe (figure 4) are noticeable. On the one hand the transition in the 20 mm pipe is less steep, the bubble velocity continuing to decrease with increasing downflow. On the other hand, for $U_c^* < U^* \lessapprox 0.02$, the shape is not strictly symmetric and the velocity departs slightly from that predicted by computations for symmetric bubbles.

3.2. *Experiments in the turbulent regime*

Figure 3 suggests that the bubble symmetry breaks for $U_c^* \approx 0.16$. However this critical velocity falls in the transitional flow regime. To extend the turbulent range we used an 80 mm pipe. The bubble velocity is plotted versus the liquid velocity in figure 7 together with the numerical predictions for symmetric bubbles in laminar and turbulent flows. Bubbles with velocity close to the numerical value are symmetric or

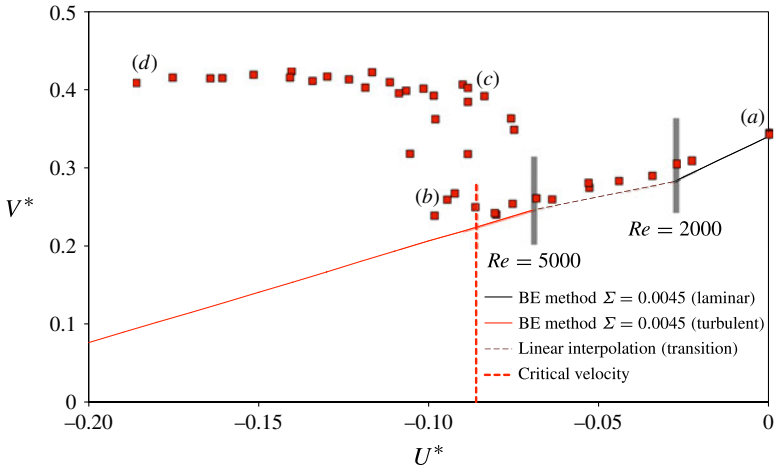

FIGURE 7. (Colour online) Bubble velocity in 80 mm pipe for water ($\Sigma = 4.5 \times 10^{-3}$, $N_v = 14 \times 10^{-6}$).

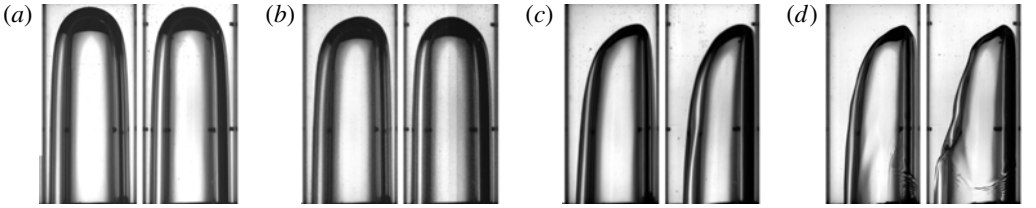

FIGURE 8. Bubble shape for the flow conditions of points (*a–d*) of figure 7.

quasi-symmetric; the others have asymmetric shapes. These observations are illustrated in figure 8 and supplementary movie 2. In still liquid the bubble is symmetric, its shape is smooth and stable (figure 8*a*). As the downflow is increased, the bubble may become either quasi-symmetric with a fluctuating tip (figure 8*b*) or asymmetric (figure 8*c*). For higher downflow (figure 8*d*) surface waves start from the tip and are swept down to the rear. However the critical velocity is not clearly defined: $U_c^* \in [-0.10, -0.07]$.

3.3. *A surprising case: the high-speed bubble*

We return now to the three fastest bubbles, the velocity of which is approximately 0.4 (figure 4). During the experiments, several other similar cases were observed but they were mistakenly rejected because of a possible measurement error. By carefully looking at the video clips we noticed that a small bubble moved near the tip of the Taylor bubble (see figure 9*a*). In the experiments, small bubbles were entrained from the rear of the long one during its ascending motion. These small bubbles were recirculated with the liquid and were trapped in the upper part of the loop in the air vent (see figure 1). However a few of them escaped from the air vent and were entrained downward with the liquid. There were some cases where the small bubble remained on the tip of the Taylor bubble, instead of moving past it as was usually the case. The capture of a small bubble by the Taylor bubble was thus possible,

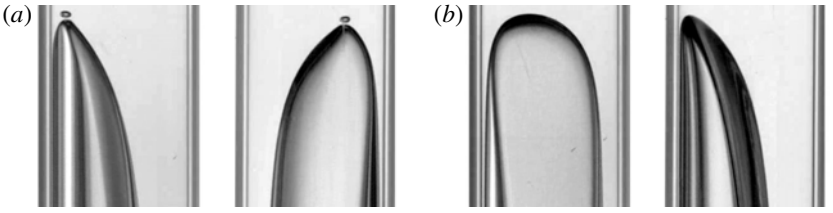

FIGURE 9. Tips of a high speed and of a regular bubble, 40 mm pipe with mixture 2. (*a*) Point (*e*) of figure 4: $U^* = -0.53$. (*b*) Point (*d*) of figure 4: $U^* = -0.56$.

though very unlikely. This is why this phenomenon was observed only in a very few experiments. Because these cases involved an element of chance, they were difficult to reproduce. A similar phenomenon was observed in the past by Maxworthy (1986), for the case of viscous fingers in Hele-Shaw cells. To increase the probability of trapping the small bubble we carried out a small modification to the experimental rig: we perforated a small air inlet in the base of the tube and injected small bubbles prior to releasing the Taylor bubble. We succeeded only a few times, enough to obtain video sequences of the bubble train.

The coupled motion of the two bubbles poses two questions. What flow conditions are behind the stable position of the small bubble? Why do the coupled bubbles of figure 9(*a*) move much faster than the regular one pictured in figure 9(*b*)?

In our opinion, the former question is the most difficult to answer. It can be shown that the trajectory of similar bubbles rising in line at large Reynolds numbers is unstable (Harper 1970) but this effect has not been studied for such a large bubble size difference. However from simple arguments it can be shown that a small bubble of diameter d and terminal velocity V_b has no stable position near the tip of a spherical cap bubble of radius R rising in still liquid at velocity V. The equilibrium position of the small bubble at a distance z_b from the stagnation point of the larger one must satisfy the force balance (Magnaudet, Rivero & Fabre 1995):

$$\boldsymbol{g} + (1 + C_M)\boldsymbol{\gamma} + \frac{3}{4} C_D \frac{|u|\boldsymbol{u}}{d} = 0, \tag{3.1}$$

where $\boldsymbol{g}$ is the buoyancy, directed upward, C_M and C_D are the added mass and drag coefficients, $\boldsymbol{\gamma}$ and $\boldsymbol{u}$ are the fluid acceleration and velocity. Near the stagnation point ($z \ll R$) the flow behaves as a biaxial straining flow, the Stokes stream function of which is $\psi = -3Vzr^2/2R$, in cylindrical coordinates (z, r). The axis-component of (3.1) leads to a second-degree equation in z_b that possesses a positive root

$$z_b = \frac{2(1 + C_M)}{3C_D} d \left[1 + \sqrt{1 + \frac{C_D}{3(1 + C_M)^2} \frac{gR^2}{dV^2}} \right], \tag{3.2}$$

resulting from the competition among drag ($\propto -z_b^2$), inertia ($\propto z_b$) and buoyancy (constant). If the bubble is shifted by a small positive (resp. negative) quantity δz_b, the difference between inertia and drag decreases (resp. increases) and thus restores the bubble position: therefore the axial position is stable. In contrast the radial position is unstable. Indeed inertia and drag are both destabilizing forces since they increase with r. In potential flow, the small bubbles must move around the spherical cap. Why they do not do so in our experiment remains unexplained.

That the coupled bubbles move much faster than a regular one might be understood as follows. Because the Taylor bubble remains in the close wake of the small one, the coupled bubbles behave as a single bubble, the tip curvature of which is that of the small bubble (figure 9*a* shows that the fast moving bubble is more pointed than the regular one of figure 9*b*). As the inviscid theory tells us (Collins *et al.* 1978; Batchelor 1987) the smaller the curvature radius the greater the bubble velocity. The Taylor bubble could thus be slaved to the small one. This interaction between a Taylor bubble and a small leading bubble has not been studied in the literature and represents an interesting phenomenon which should be addressed in future investigations.

4. Discussion

4.1. *Symmetric bubbles*

Axisymmetric bubbles in flowing liquid have been extensively investigated, especially at high Reynolds number and small surface tension. However the results, be they analytical, experimental or numerical, are limited to upward flow. The present experimental results fill the gap for downward flow at least for the bubble velocity. But for the tip curvature, it was difficult to get an accurate value from the present experiments. This is why we performed additional numerical experiments to complement the present experimental results. For such free-surface flow at high Reynolds number where the viscosity can be ignored, the BE method has proved to be both fast and accurate. A summary of the results obtained from the method of Ha Ngoc & Fabre (2006) is given in appendix A.

The theory of Collins *et al.* (1978) shows that the bubble dynamics is primarily controlled by the flow near the bubble tip. Thus the velocity profile may be approximated near the axis by the truncated series

$$u^*(r^*) \approx u_0^* - \tfrac{1}{2}\Omega_0^* r^{*2}, \tag{4.1}$$

where $\Omega = -\omega/r$, ω being the vorticity. Note that with this definition Ω_0^* and u_0^* have the same sign, positive for upward flow and negative for downward flow; note also that the above equation is exact for laminar flow. Equation (4.1) implies that V^* and R^* should depend on u_0^* and Ω_0^* regardless of whether the flow is laminar or turbulent.

Therefore, to unify the results obtained from various velocity distributions, V^* should be plotted against u_0^* rather than against U^* as (1.1) might suggest. The bubble velocity V^* is shown in figure 10(*a*) for two different Σ. Over the range of liquid velocities considered in the figure, V^* is a linear function of u_0^*: this function equally applies to upward and downward flows. The slope $C_1 = C_0 U/u_0$ weakly depends on the surface tension parameter (see table 2); it may also depend on Ω_0^*. It decreases when Σ increases and for $\Sigma < 0.02$ it is independent of the flow regime. Moreover C_1 is always smaller than unity contrary to what most of the analytical studies suggest: for example the solution in cylindrical harmonics of Collins *et al.* (1978) and Bendiksen (1985) leads to $C_1 = 1.13$. The solid lines of figures 3, 4, 6 and 7 were calculated with (1.1) and the values of $C_1 = C_0 U/u_0$ and C_∞ given in table 2: they are in good agreement with the experimental values.

The curvature radius at the bubble tip, R^*, plays a major role in the bubble stability (Figueroa-Espinoza & Fabre 2011). Like V^*, R^* should be a function of u_0^* and Ω_0^*. However it is a frame-invariant quantity and, as such, it should not depend on u_0^* but solely on Ω_0^*. Because $\Omega_0^* = 2u_0^*$ in laminar flow, it could be argued that this question is irrelevant but for a turbulent velocity distribution (see appendix A) $\Omega_0^* = 2\gamma u_0^*$

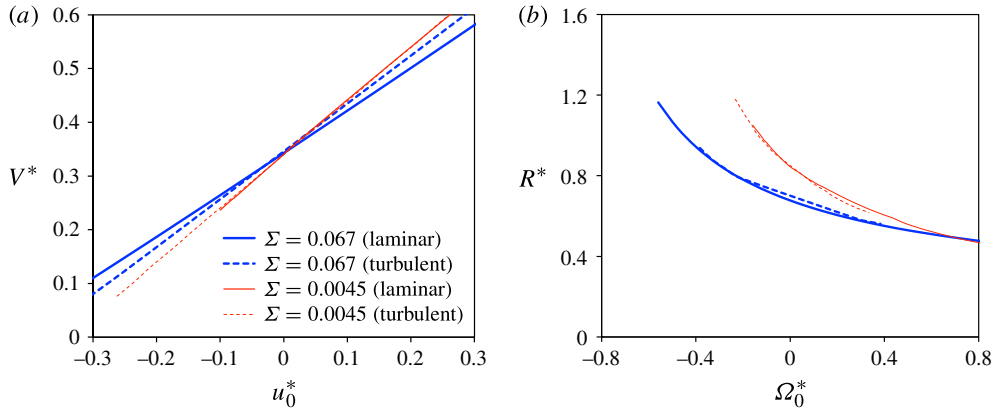

FIGURE 10. (Colour online) (*a*) Velocity and (*b*) curvature radius from the method of Ha Ngoc & Fabre (2006).

Σ	C_1 laminar	C_1 turbulent	C_∞	R^* $U^*=0$
0.067	0.79	0.89	0.346	0.68
0.038	0.89	0.94	0.346	0.69
0.018	0.97	0.97	0.345	0.72
0.010	0.99	0.99	0.343	0.74
0.0045	0.99	1.00	0.340	0.84

TABLE 2. Velocity and curvature parameters determined from the BE method of Ha Ngoc & Fabre (2006).

with $\gamma < 1$. R^* is plotted versus Ω_0^* in figure 10(*b*) for two values of Σ. Negative (resp. positive) Ω_0^* corresponds to downward (resp. upward) flow. It should be noted that the bubble tip flattens out when Ω_0^* decreases. This phenomenon is accentuated in downward flow for which the curvature radius at the tip may be greater than the tube diameter ($R^* > 1$). The surface tension also has a great influence on the curvature radius, especially in downward flow: the smaller Σ the greater R^*. As one expects that 'the bubble is gravitationally unstable for sufficiently large radii of curvature' (Batchelor 1987) it should be more fragile in downward flow and even more so if the surface tension is smaller.

4.2. *Asymmetric bubbles*

The present experimental results are combined in figure 11, using the axis velocity u_0^* to characterize the liquid motion. A grey line has been added to show the region of symmetric bubbles. Although surface tension has a marginal influence on the dynamics of symmetric bubbles, it has a significant influence on asymmetric bubbles, no matter how small Σ might be. A similar result has been observed in channel flow by Figueroa-Espinoza & Fabre (2011, figure 8). The results of figure 11 raise two important issues: the occurrence of symmetry breaking and the dynamics of asymmetric bubbles.

In the transition from symmetric to asymmetric bubbles the viscosity has no influence whenever the viscosity parameter N_ν is small enough (see for example figure 5). Under the inviscid assumption the dynamics of a symmetric bubble in

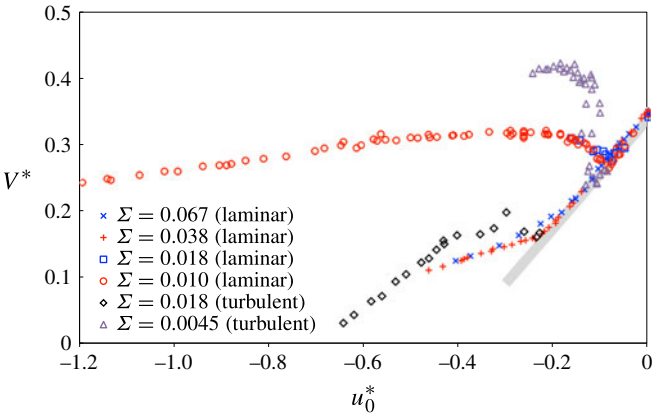

FIGURE 11. (Colour online) Summary of the present results (the grey line indicates the symmetric domain).

Flow regime	Σ	$-U_c^*$	$-\Omega_{0,c}^*$	R_c^*
Laminar	0.011	0.045	0.18	0.88
Laminar	0.040	0.110	0.44	1.15
Laminar	0.018	0.038	0.15	0.85
Laminar	0.067	0.090	0.36	0.90
Turbulent	0.018	0.160	0.19	0.90
Turbulent	0.0045	0.086	0.12	0.97

TABLE 3. Critical conditions at symmetry breaking.

rotational flow depends on u_0^*, Σ and Ω_0^* but for the reasons mentioned in § 4.1 the transition should not depend directly on u_0^*. Thus Ω_0^* should be the correct bifurcation parameter.

It may be difficult to determine the critical flow condition especially when the surface tension is not small enough or when the flow is turbulent: for $\Sigma > 0.01$ the transition is too smooth and for turbulent flow the points are too scattered (see figure 11) for the critical conditions to be determined accurately. Moreover, as tap water was used one cannot rule out its contamination. The critical conditions given in table 3 are thus determined with some uncertainty. In particular Ω_0^* was determined from the analytical velocity profile used by Collins *et al.* (1978) as detailed in appendix A. Figure 12(*a*) shows that most of the present results fall into the strip

$$\Omega_{0,c}^* = -(7.5\Sigma + 0.06) \pm 0.07, \tag{4.2}$$

the width of which may result from the uncertainty in estimating the bifurcation. It is remarkable that the above equation applies to both the laminar and turbulent results. It is still more remarkable that it also applies to the results in channel flow (numerical experiments of Figueroa-Espinoza & Fabre 2011). Coincidence? A theoretical investigation would be helpful to address this issue. The only attempt is that of Lu & Prosperetti (2006) which leads to $U_c = 0.135$, i.e. to $\Omega_{0,c}^* = 0.54$, from a linear stability analysis for $\Sigma = 0$. Unfortunately this result disagrees with (4.2), perhaps because the analytical solution of the unperturbed flow, a truncated series of

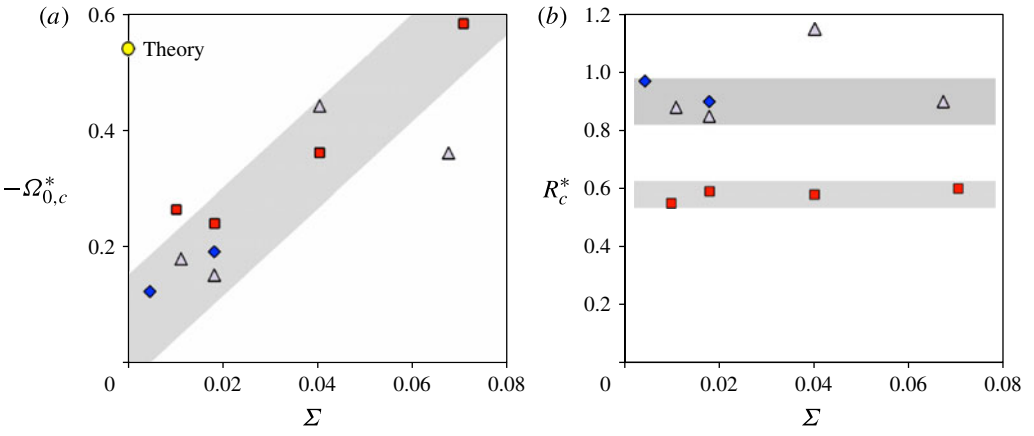

FIGURE 12. (Colour online) (*a*) Critical value of Ω_0 and (*b*) curvature radius at criticality, for: laminar flow (△), turbulent flow (♦), two-dimensional numerical simulation of Figueroa-Espinoza & Fabre (2011) (■), and linear stability analysis of Lu & Prosperetti (2006) (○). Grey strips correspond to (4.2) for (*a*) and to $R^*_c \approx 0.6$ and 0.9 for (*b*).

cylindrical harmonics, fails to predict the bubble velocity and the curvature radius accurately.

For channel flow, Figueroa-Espinoza & Fabre (2011) observed that the curvature radius of a symmetric bubble is smaller than the critical radius $R^*_c \approx 0.6$ (see figure 12*b*). A similar conclusion can be drawn from the present results: bifurcation occurs at $R^*_c \approx 0.9$ whether the velocity distribution is laminar or turbulent. This suggests that the symmetry cannot be maintained when the bubble tip is too flat. The similarity between channel and tube flow is not only qualitative, it is also quantitative since $R^*_{c,tube}/R^*_{c,channel} = 3/2$, the ratio between the dimensions of three-dimensional and two-dimensional flows.

The excess velocity ΔV^*, defined as the difference $V^* - (C_1 u^*_0 + C_\infty)$ between the actual velocity and that of fictitious symmetric bubbles, characterizes the behaviour of asymmetric bubbles. This excess is plotted versus Ω^*_0 in figure 13(*a*) and the channel results, determined from the data of Figueroa-Espinoza & Fabre (2011), are shown in figure 13(*b*). The similarity between the tube and channel cases is remarkable for laminar flow. When Ω^*_0 decreases below $\Omega^*_{0,c}$, ΔV^* increases and, after a transition region, the slope $\mathrm{d}\Delta V^*/\mathrm{d}\Omega^*_0$ becomes nearly constant and depends little on Σ unlike in the transition region in which $\mathrm{d}\Delta V^*/\mathrm{d}\Omega^*_0$ is very sensitive to Σ. At the present time, a comprehensive theory of the dynamics of asymmetric bubbles is lacking. Because of the complexity of the three-dimensional case, a two-dimensional approach should be tried.

5. Conclusion

The problem of a single Taylor bubble rising in counter-current flow was addressed, by means of a series of experiments in 20, 40 and 80 mm diameter tubes. With these diameters the surface tension parameter could be varied by a factor of 16. Different mixtures of water and glycerol were prepared to vary the viscosity and to control the velocity profile through the flow regime (laminar and turbulent). This velocity profile, which has a major influence upon the bubble dynamics, was measured by

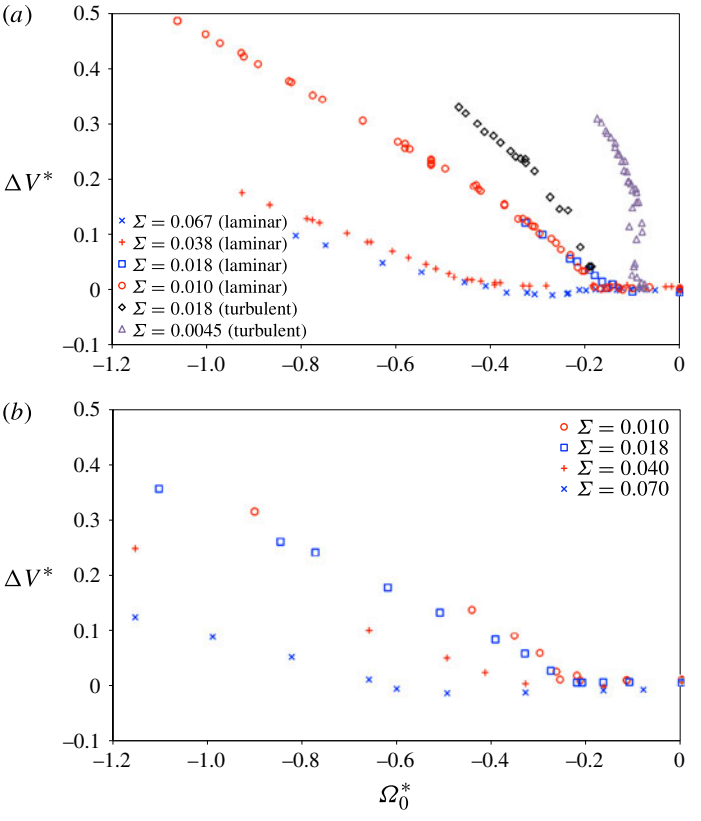

FIGURE 13. (Colour online) Excess velocity of asymmetric bubbles: (*a*) experiments in a tube; (*b*) simulations in a channel (Figueroa-Espinoza & Fabre 2011).

PIV. Taylor bubbles were formed by injecting a given volume of air into a separate chamber. The experiments were carried out at constant volume to eliminate errors due to the expansion of the bubble while rising. The bubble velocity was carefully measured and its shape was captured using a high-speed camera. Confirming previous investigations in downward liquid flow (Griffith & Wallis 1961; Nicklin *et al.* 1962; Martin 1976), it was observed that below some critical liquid velocity ($U^* < U_c^* < 0$), the flow symmetry is broken and the bubble changes its shape to rise in an eccentric motion. The bubble tip moves close to the tube wall; its shape changes to resemble that of a wedge, trying to avoid the fastest moving liquid at the centre of the tube. As the liquid velocity increases, the tip eccentricity also increases, as, presumably, does its mean curvature. The critical velocity was determined for each value of the surface tension parameter Σ; however, for the turbulent regime there exists some uncertainty due to the unsteady character of the flow.

Additional numerical experiments were performed using the BE method of Ha Ngoc & Fabre (2006) to determine the velocity and shape that the Taylor bubble would have if it were symmetric.

The results of physical and numerical experiments as well as theoretical considerations can be summarized as follows.

(*a*) From dimensional analysis, the dynamics of Taylor bubbles at high Reynolds number is shown to depend on the fluid properties Σ and flow conditions, i.e. the velocity u_0^* and the vorticity to radius ratio $\Omega_0^* = 2\gamma u_0^*$ on the axis, with $\gamma(\leqslant 1)$ characterizing the velocity distribution.

(*b*) Whenever the bubble is symmetric, the law (1.1) of Nicklin *et al.* (1962) that expresses V^* as a linear function of U^* applies equally to upward and downward flows. On using u_0^* rather than U^*, the law extends to various velocity profiles, i.e. laminar and turbulent. The bubble velocity V^* is weakly sensitive to Σ. The present results show that the theoretical solutions (Collins *et al.* 1978; Bendiksen 1985) overestimate the velocity in laminar flow (they predict $C_1 = 1.13$ for $\Sigma = 0$ whereas the values of table 2 show that C_1 is always smaller than unity). As a consequence they overestimate the curvature radius at the nose. Unlike V^* the curvature radius at the tip R^* (that plays a major role in the bubble stability) is very sensitive to Σ. The bubble tip flattens out when Ω_0^* decreases. This phenomenon is accentuated in downward flow for which the curvature radius at the tip may be greater than the tube diameter.

(*c*) From dimensional arguments it has been shown that the critical parameter is Ω_0^*. Its value increases with increasing Σ. It is remarkable that the results obtained (i) in channel and pipe flows and (ii) for laminar and turbulent profiles, display almost the same trend as that represented by (4.2) and shown in figure 12(*a*). In addition, symmetry breaking is shown to occur above a critical curvature radius at the bubble tip, i.e. for $R_c^* > 0.9$ in tube flow and $R_c^* > 0.6$ in plane flow.

(*d*) The three-dimensional results in tubes and the two-dimensional numerical simulations of Figueroa-Espinoza & Fabre (2011) in channels are remarkably similar. A theoretical study of two-dimensional channel flow should therefore be worthwhile, and has the added advantage that it should be easier to perform.

(*e*) A very unexpected phenomenon was observed a few times at large liquid counter-current flow: an asymmetric Taylor bubble slaved to a small leading one. Although small, the leading bubble shelters the Taylor bubble and imposes its curvature on the bubble pair. As a result, the coupled bubbles rise at a speed that is even greater than that of a Taylor bubble in stagnant liquid.

Acknowledgements

We acknowledge the support of TOTAL S.A. We also thank F. Luck and D. Larrey for interesting discussions and for their involvement throughout the duration of the study. We are grateful to H. Ha-Ngoc and A. Pedrono for their contribution to the results of appendix A.

Supplementary movies

Supplementary movies are available at http://dx.doi.org/10.1017/jfm.2014.429.

Appendix A. Axisymmetric bubbles: velocity and tip curvature

The numerical solution for axisymmetric bubbles is obtained from a code developed by Ha Ngoc & Fabre (2006) that computes the irrotational or rotational inviscid two-dimensional flow of a liquid past a bubble at large Reynolds number. For axisymmetric flow in a tube, the equation of the Stokes stream function ψ satisfies

$$\frac{\partial^2 \psi}{\partial z^{*2}} + \frac{\partial^2 \psi}{\partial r^{*2}} = \frac{1}{r^*}\frac{\partial \psi}{\partial r^*} + r^{*2}\Omega^*(\psi), \tag{A 1}$$

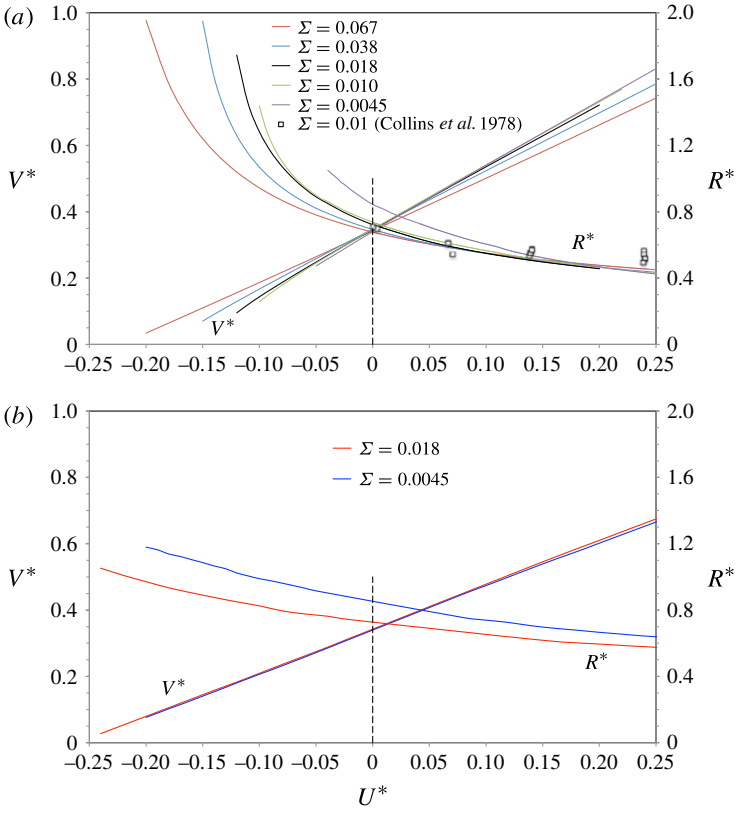

FIGURE 14. Velocity and curvature radius at the bubble tip: (*a*) laminar profile; (*b*) turbulent profile.

where $\Omega^* = -\omega^*/r^*$, and ω^* is the vorticity. This equation is solved in the (z^*, r^*) plane by a boundary element method with an iterative loop for the terms of the right-hand side. It is solved together with the Bernoulli equation at the interface and a prescribed velocity profile far upstream. The bubble shape and its velocity are determined as part of the solution.

For the present calculations, we adopted the velocity distribution used by Collins *et al.* (1978) and Bendiksen (1985):

$$u^*(r^*) = u_0^*[1 - \gamma r^{*2} - (1-\gamma)r^{*2n}], \tag{A 2}$$

which gives the Ω^* distribution

$$\Omega^*(r^*) = 2u_0^*[\gamma + n(1-\gamma)r^{*2(n-1)}], \tag{A 3}$$

in which γ is chosen to fit the desired profile:

$$\gamma = \begin{cases} 1 & \text{for laminar profile,} \\ 1.51/\log_{10}(1.23Re) & \text{for turbulent profile,} \end{cases} \tag{A 4}$$

with $Re = UD/\nu$, the Reynolds number of the carrying fluid. The exponent n depends on Re through the friction law:

$$n = (\gamma - 1)\left(\frac{\log_{10} Re - 0.74}{\log_{10} Re + 0.31} - 1 + \frac{\gamma}{2}\right)^{-1} - 1. \tag{A 5}$$

Although the turbulent profile from (A 2) or (A 3) is questionable near the tube wall, it is accurate within a cylinder of approximately $0.8D$ and thus adequate for the present purpose.

The mean-to-maximum velocity ratio is expressed as

$$\frac{U^*}{u_0^*} = 1 - \frac{\gamma}{2} - \frac{1-\gamma}{n+1}. \tag{A 6}$$

Some numerical results in upward flow have already been obtained by Ha Ngoc & Fabre (2004) with this code. They have been complemented in both upward and downward flow for $\Sigma = 0.067$, 0.038, 0.018, 0.010, 0.0045. Figure 14(*a*) shows the velocity V^* and the curvature radius R^* for laminar profiles and $\Sigma = 0.067$, 0.038, 0.018, 0.010, 0.0045, figure 14(*b*) for turbulent profiles and $\Sigma = 0.018$, 0.0045.

REFERENCES

Batchelor, G. K. 1987 The stability of a large gas bubble rising through liquid. *J. Fluid Mech.* **184**, 399–422.

Bendiksen, K. H. 1985 On the motion of long bubbles in vertical tubes. *Intl J. Multiphase Flow* **11**, 797–812.

Canny, J. 1986 A computational approach to edge detection. *IEEE Trans. Pattern Anal. Mach. Intell.* **8** (6), 679–698.

Collins, R., de Moraes, F., Davidson, J. F. & Harrison, D. 1978 The motion of large bubbles rising through liquid flowing in a tube. *J. Fluid Mech.* **89**, 497–514.

Fabre, J. & Liné, A. 1992 Modeling of two-phase slug flow. *Annu. Rev. Fluid Mech.* **24**, 21–46.

Figueroa-Espinoza, B. & Fabre, J. 2011 Taylor bubble moving in a flowing liquid in vertical channel: transition from symmetric to asymmetric shape. *J. Fluid Mech.* **679**, 432–454.

Griffith, P. & Wallis, G. B. 1961 Two phase slug flow. *Trans. ASME: J. Heat Transfer* **83**, 307–320.

Ha Ngoc, H. & Fabre, J. 2004 The velocity and shape of 2D long bubbles in inclined channels or in vertical tubes. Part II: in a flowing liquid. *Multiphase Sci. Technol.* **16** (1–3), 189–204.

Ha Ngoc, H. & Fabre, J. 2006 A boundary element method for calculating the shape and velocity of two-dimensional long bubble in stagnant and flowing liquid. *Engng Anal. Bound. Elem.* **30**, 539–552.

Harper, J. F. 1970 On bubbles rising in line at large Reynolds numbers. *J. Fluid Mech.* **41** (4), 751–758.

Lu, X. & Prosperetti, A. 2006 Axial stability of Taylor bubbles. *J. Fluid Mech.* **568**, 173–192.

Magnaudet, J., Rivero, M. & Fabre, J. 1995 Accelerated flows past a rigid sphere or a spherical bubble. Part I: steady straining flow. *J. Fluid Mech.* **284**, 97–135.

Martin, C. S. 1976 Vertically downward two-phase slug flow. *Trans. ASME J. Fluids Engng* **98**, 715–722.

Maxworthy, T. 1986 Bubble formation, motion and interaction in a Hele-Shaw cell. *J. Fluid Mech.* **173**, 95–114.

Nicklin, D. J., Wilkes, J. O. & Davidson, J. F. 1962 Two phase flow in vertical tubes. *Trans. Inst. Chem. Engrs* **40**, 61–68.